# Numerical assessment of a double-acting offshore vessel's performance in level ice with experimental comparison

Biao Su [a,*], Roger Skjetne [a], Tor Einar Berg [b]

[a] Department of Marine Technology, NTNU, Trondheim, NORWAY

[b] MARINTEK, Trondheim, NORWAY

**Abstract**

In this paper a numerical model is used to investigate the level ice performance of a double-acting intervention vessel, and the results are compared with a limited set of experimental data. The icebreaking capability and maneuverability in level ice are analyzed by evaluating the behavior of the vessel when it is running both ahead and astern. The simulated icebreaking patterns, $h$ - $v$ curves, and turning circles in different modes of operation are discussed and compared partly with the corresponding ice model tests. The simulation results can supplement the experimental data by providing more information about the vessel's maneuverability in level ice and identifying the physical foundation for the exhibited performance of the vessel. The paper also presents the implementation of a random crack size model for more realistic icebreaking behavior, giving more consistent evaluation of the ship's performance in various ice conditions.

**Keywords:**

Double-acting vessel; numerical model; icebreaking capability; ship maneuverability; ice model test

## 1. Introduction

Since the beginning of the 1990s, the major development of ice-going ships has been the use of podded propellers in ice with double-acting vessels (Jones, 2004). The idea is to design an efficient icebreaking stern for the vessel while keeping an efficient open-water bow. During these years a number of vessels have been designed and built according to the double-acting principle. Vocke et al. (2011) presented a recent review of the experiences gained from realized projects where the most relevant milestones in double-acting vessel developments were summarized. These vessels were first tested and studied in the ice model basin to get the best possible design features. Many operational experiences have also been gained through full-scale ice trials and practical operations of the vessels.

The double-acting principle is of interest to the offshore industry as the oil and gas explorations are moving further north. In collaboration with several research institutes and companies, MARINTEK recently completed a project to develop a vessel (the CIVArctic vessel) for all-year intervention work on subsea oil and gas installations in the northeastern part of the Barents Sea. As the vessel will be operating and transiting in open waters for most of its working time, the design focus was initially on open-water performance. An efficient

---

∗ Corresponding author. Tel.: +47 73551113; fax: +47 73595697; e-mail address: biao@ntnu.no (B. Su).

icebreaking stern was then designed for operation in moderate first-year level ice. A series of open-water and ice model tests have been carried out to verify this design (Berg et al., 2013).

In the present paper a numerical model is applied to evaluate the level ice performance of the CIVArctic vessel. In general it should be mentioned that level ice breaking takes only a small fraction of the total operating time of the vessel. The reason why the level ice is often considered is that the design ice conditions are defined in most ice class rules (e.g. Finish–Swedish Ice Class Rules) by using the equivalent level ice thickness. Analysis of the hull damages caused by ice shows that this definition gives a reasonable estimate of the severity of ice conditions (Riska, 2007). For a more robust design, the CIVArctic vessel was also tested in floe ice and ice ridges; however, this paper only focuses on the level-ice performance and mainly describes the numerical studies with a comparison to experimental test results. The icebreaking capability and maneuverability in level ice are analyzed by evaluating the behavior of the vessel when it is running both ahead and astern. The results of the comparison also identify the physical foundation for the exhibited performance. Another contribution of this paper is the implementation of a random crack size in the modeling of icebreaking. This will give a more consistent evaluation of the ship's performance in various ice conditions.

## 2. Numerical model

As shown by the illustration in Figure 1, the ice forces encountered by a ship transiting level ice depend primarily on the icebreaking and displacement processes. First the ice sheet touches the hull, and crushing occurs. This load will increase with the contact area until the ice sheet fails some distance away from the interaction zone. The failure mechanisms are mainly governed by the interaction geometry and ice material properties involved. For inclined planes, this usually means a bending failure. After the ice floe has been broken from the ice sheet, the advancing ship forces it to rotate, submerge, and slide along the hull. In some hull zones, typically at the shoulders and midship with large slope angles, crushing may be the only failure mode. A relative heading towards the ice sheet heavily exposing these hull sections will cause enlarged resistance.
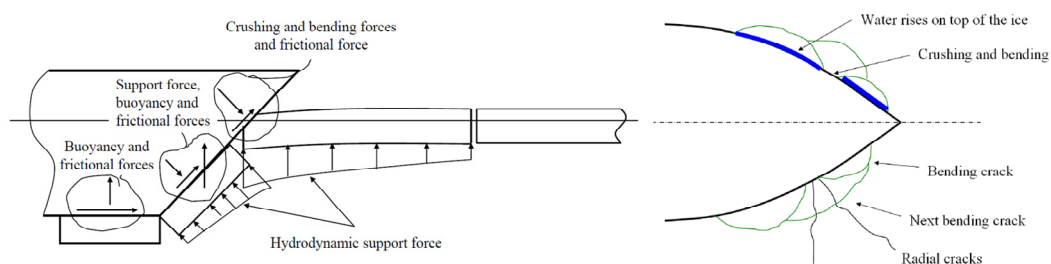


Figure 1. Illustration of the ice–hull interaction process (Source: Riska, 2010).

Relevant examples of research on numerical modeling of ice–hull interaction and ship maneuvering in level ice can be found in Valanto (2001), Liu et al. (2006), Martio (2007), Nguyen et al. (2009), Sawamura et al. (2010), Lubbad and Løset (2011), Tan et al. (2013), and Metrikin et al. (2013). In this paper, the validated partly empirical numerical model presented in Su et al. (2010a) is applied to investigate the icebreaking capability and maneuverability of the CIVArctic vessel in level ice. A 2D simulation program has been developed to reproduce the observed icebreaking patterns and the continuous icebreaking forces imposed by a level ice sheet, where the

ice has uniform or randomly varying thickness and strength properties. The numerical method for the realization of the physical process of icebreaking can be found in Su et al. (2010a, 2011), while the simulation of ship maneuvering is mainly described herein.

## 2.1 Equations of ship's motion

Figure 2 illustrates the numerical ice−hull interaction model, which enables simulations of ice maneuvering by solving the three-degrees-of-freedom differential motion equations for surge, sway, and yaw:

$$\left(\mathbf{M}+\mathbf{A}\right)\cdot\ddot{\mathbf{x}}(t)+\mathbf{B}\cdot\dot{\mathbf{x}}(t)+\mathbf{C}\cdot\mathbf{x}(t)=\mathbf{F}(t) \tag{1}$$

where $\mathbf{M}$, $\mathbf{A}$, $\mathbf{B}$, and $\mathbf{C}$ are the rigid body mass, added mass, damping, and restoring force matrices, $\mathbf{x}=\begin{bmatrix} x & y & \psi \end{bmatrix}^{\mathrm{T}}$ is the displacement vector (surge, sway, and yaw) expressed as a function of time $t$, $\dot{\mathbf{x}}$ and $\ddot{\mathbf{x}}$ are, respectively, the first and second time derivatives of $\mathbf{x}$ (velocity and acceleration), and $\mathbf{F}=\begin{bmatrix} F_x & F_y & M_z \end{bmatrix}^{\mathrm{T}}$ is the force/moment vector.

The added mass and damping matrices are calculated in open water without considering the effect of ice. The contributions from wind and waves are neglected as minor forces to the ice load.
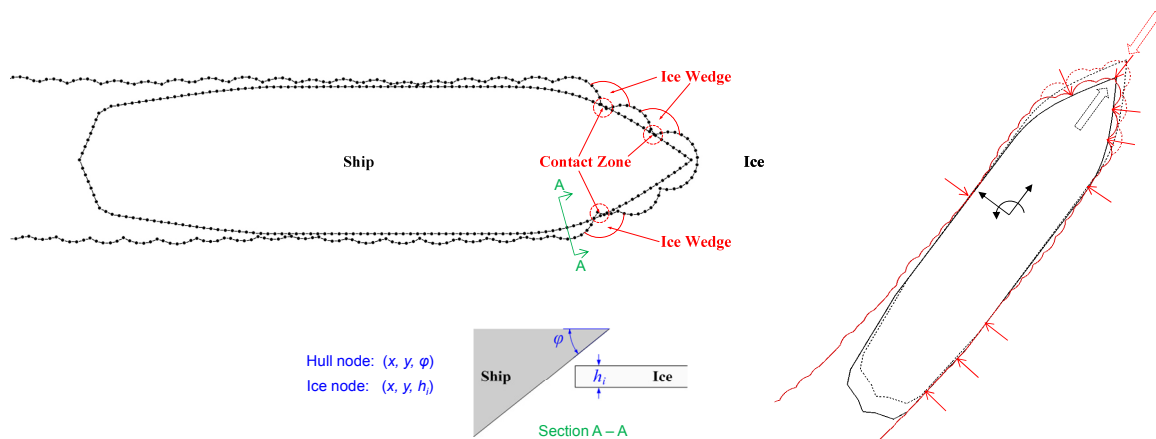


Figure 2. Illustration of the numerical ice–hull interaction model (Su et al., 2010a).

## 2.2 Force decomposition

In order to evaluate the forces encountered by a ship transiting in level ice, one of the basic assumptions that have commonly been accepted is that the total ice resistance can be taken as the superposition of several force components, that is, icebreaking force, ice floe rotation and submergence force, and friction force associated with ice contact. However, this assumption is questionable since the force components could be "complicatedly entangled in each other" (Enkvist et al., 1979; see also Kjerstad et al., 2014, where these phenomena are discussed further, especially the interaction between the vessel and the accumulated ice masses, which effectively increases the total mass of the affected system). Moreover, since open-water resistance is usually very small compared to ice resistance at icebreaking speeds, the coupling between them could be neglected without causing significant errors. Thus, we assume that the open-water resistance and the pure ice resistance are also separable (as described in Riska et al., 1997).

Based on this superposition principle, the force/moment vector is then decomposed as:

$$\mathbf{F} = \mathbf{F}_p + \mathbf{F}_{brk} + \mathbf{F}_{sbmg} + \mathbf{F}_{ow} + \mathbf{F}_{Euler} \tag{2}$$

where $\mathbf{F}_p$ is the propulsion force, $\mathbf{F}_{brk}$ is the icebreaking force, $\mathbf{F}_{sbmg}$ is the ice forces induced during the displacement process (i.e., rotating, submerging, and sliding the broken ice pieces), $\mathbf{F}_{ow}$ is the open water force, and $\mathbf{F}_{Euler}$ is a fictitious force (i.e., the Coriolis and centripetal force) induced by a non-uniformly rotating frame (i.e., the body-fixed frame) relative to the inertial frame.

Since the focus of this numerical model is on the icebreaking process, the icebreaking force $\mathbf{F}_{brk}$, which is the immediate cause of the formation of the icebreaking pattern, is calculated by simulating the continuous icebreaking patterns and integrating the local icebreaking forces along the waterline (as shown in Figure 2), while other force components are estimated by some well-proven theoretical or semi-empirical formulas. For example, the open water force $\mathbf{F}_{ow}$ is calculated by the crossflow theory given in Faltinsen (1990), $\mathbf{F}_{sbmg}$ is calculated by following the force superposition principle given in Lindqvist (1989), and the propulsion force $\mathbf{F}_p$ is estimated by the net thrust in ice (Juva and Riska, 2002).

### 2.3 Numerical integration

A step-by-step numerical integration method is applied to solve the equations of the ship's motion. According to Newmark's method (Newmark, 1959), the general integral equations are:

$$\dot{\mathbf{x}}(t_{k+1}) = \dot{\mathbf{x}}(t_k) + (1 - \lambda) \cdot \ddot{\mathbf{x}}(t_k) \cdot \Delta t + \lambda \cdot \ddot{\mathbf{x}}(t_{k+1}) \cdot \Delta t$$

$$\mathbf{x}(t_{k+1}) = \mathbf{x}(t_k) + \dot{\mathbf{x}}(t_k) \cdot \Delta t + \left( \frac{1}{2} - \beta \right) \cdot \ddot{\mathbf{x}}(t_k) \cdot \Delta t^2 + \beta \cdot \ddot{\mathbf{x}}(t_{k+1}) \cdot \Delta t^2 \tag{3}$$

These equations are obtained by a Taylor-series expansion in which the residual term is approximated by the quadrature formula. The weighting terms $\lambda$ and $\beta$ are free parameters in the quadrature formula that are determined by the requirements related to stability and accuracy. If a linear acceleration is assumed within the time interval $\Delta t$, we choose $\lambda = \frac{1}{2}$ and $\beta = \frac{1}{6}$, and (3) becomes:

$$\dot{\mathbf{x}}(t_{k+1}) = \dot{\mathbf{x}}(t_k) + \frac{1}{2} \ddot{\mathbf{x}}(t_k) \cdot \Delta t + \frac{1}{2} \ddot{\mathbf{x}}(t_{k+1}) \cdot \Delta t$$

$$\mathbf{x}(t_{k+1}) = \mathbf{x}(t_k) + \dot{\mathbf{x}}(t_k) \cdot \Delta t + \frac{1}{3} \ddot{\mathbf{x}}(t_k) \cdot \Delta t^2 + \frac{1}{6} \ddot{\mathbf{x}}(t_{k+1}) \cdot \Delta t^2 \tag{4}$$

where

$$\ddot{\mathbf{x}}(t_{k+1}) = (\mathbf{M} + \mathbf{A})^{-1} (\mathbf{F}(t_{k+1}) - \mathbf{B} \cdot \dot{\mathbf{x}}(t_{k+1}) - \mathbf{C} \cdot \mathbf{x}(t_{k+1})) \tag{5}$$

This is a popular method resulting in continuity in the acceleration, velocity, and displacement. By inserting (5) into (4), we get the explicit form:

$$\mathbf{x}(t_{k+1}) = \left(\frac{6}{\Delta t^2}(\mathbf{M}+\mathbf{A}) + \frac{3}{\Delta t}\mathbf{B}+\mathbf{C}\right)^{-1} \cdot \left(\mathbf{F}(t_{k+1}) + (\mathbf{M}+\mathbf{A})\cdot \mathbf{a}_k + \mathbf{B}\cdot \mathbf{b}_k\right) \qquad (6)$$

where

$$\mathbf{a}_k = \frac{6}{\Delta t^2}\mathbf{x}(t_k) + \frac{6}{\Delta t}\dot{\mathbf{x}}(t_k) + 2\ddot{\mathbf{x}}(t_k)$$

$$\mathbf{b}_k = \frac{3}{\Delta t}\mathbf{x}(t_k) + 2\dot{\mathbf{x}}(t_k) + \frac{1}{2}\ddot{\mathbf{x}}(t_k)\cdot \Delta t \qquad (7)$$

## 2.4 Iteration and convergence criteria

As shown in (6), the force/moment vector at time step $k+1$, that is, $\mathbf{F}(t_{k+1})$, is unknown at time step $k$ due to the interdependence between the ice loads and the ship's motion. Thus, iterations are performed at each time step until an acceptable accuracy is achieved. Herein, the convergence criterion is based on the variation of the force/moment vector from iteration step $i$ to iteration step $i+1$, given by:

$$\frac{\left|\mathbf{F}(t_{k+1})_{i+1} - \mathbf{F}(t_{k+1})_i\right|}{\left|\mathbf{F}(t_{k+1})_i\right|} < \varepsilon \qquad (8)$$

where $\varepsilon$ is a small, positive number of the order of $10^{-3}$.

The above numerical procedure is implemented into a FORTRAN program, which is illustrated by the flowchart given in Figure 3. At each time step, the force vector is firstly assumed to be the same as in the previous step. It is then updated by solving the equations of the ship's motion and integrating the local contact forces between the ice and hull. If the updated force vector satisfies the convergence criterion defined in (8), it will be accepted as the final solution for the present time step. Otherwise it will be used to resolve the equations of the ship's motion and to recalculate the contact forces between the ice and hull. The purpose of introducing this iterative procedure is to find a balance between the penetration of the vessel into ice and the resulting ice forces. It can be expected that the broken ice channel formed at one moment will have a cumulative effect on the following icebreaking process, especially during ship maneuvering (Su et al., 2010b). Thus, the continuous icebreaking process can be more correctly reproduced by applying an iterative procedure for the determination of the ice load and ship's motion at each time step.
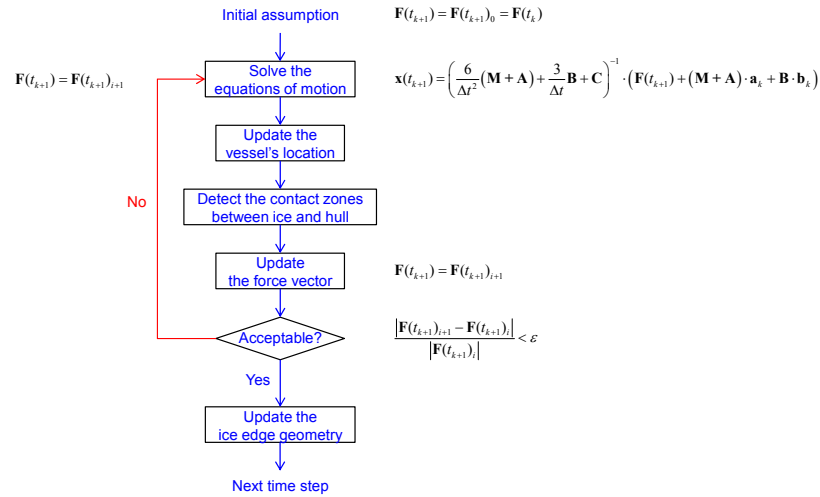
At the top of the flow chart:

Initial assumption — $\mathbf{F}(t_{k+1}) = \mathbf{F}(t_{k+1})_0 = \mathbf{F}(t_k)$

$\mathbf{F}(t_{k+1}) = \mathbf{F}(t_{k+1})_{i+1}$

Solve the equations of motion — $\mathbf{x}(t_{k+1}) = \left(\dfrac{6}{\Delta t^2}(\mathbf{M}+\mathbf{A}) + \dfrac{3}{\Delta t}\mathbf{B} + \mathbf{C}\right)^{-1} \cdot \left(\mathbf{F}(t_{k+1}) + (\mathbf{M}+\mathbf{A})\cdot \mathbf{a}_k + \mathbf{B}\cdot \mathbf{b}_k\right)$

Update the vessel's location

Detect the contact zones between ice and hull

Update the force vector — $\mathbf{F}(t_{k+1}) = \mathbf{F}(t_{k+1})_{i+1}$

Acceptable? — $\dfrac{\left|\mathbf{F}(t_{k+1})_{i+1} - \mathbf{F}(t_{k+1})_i\right|}{\left|\mathbf{F}(t_{k+1})_i\right|} < \varepsilon$

No

Yes

Update the ice edge geometry

Next time step

Figure 3. Flow chart of the numerical procedure.

## 3. Ice model test and numerical modeling for the CIVArctic vessel

The CIVArctic vessel is mainly designed for open-water operations and the double-acting principle ensures icebreaking capabilities with the stern. Table 1 features the main dimensions of the vessel. The main propulsion of the vessel is two azimuth propulsors of 5 MW each. The propeller blades of these are reinforced to handle ice milling during ice interaction. To achieve feasible DP station-keeping capability, the vessel is also equipped with two retractable azimuth thrusters and two tunnel thrusters in the foreship.

Table 1. Main dimensions of the CIVArctic vessel.

| Parameters | Full-scale Value | Model-scale Value |
|---|---|---|
| Length overall | 121.8 m | 5.0 m |
| Length between perpendiculars | 109.3 m | 4.5 m |
| Breadth moulded | 24.0 m | 1.0 m |
| Depth of main deck | 10.5 m | 0.43 m |
| Maximum scantling draught midship | 8.0 m | 0.33 m |
| Design draught | 6.5 m | 0.27 m |

### 3.1 Ice model test

To evaluate the vessel's ice performance, a series of model experiments were carried out in the Aker Arctic ice basin during May 2011 (Leiviskä, 2011). The main parameters of the ice basin are given in Table 2 (Wilkman et al., 2010). The tests included three days of forward ice-keeping performance, one day of ice maneuvering (see Figure 4), and three days of station-keeping in ice. The vessel model, having a scale of 1:24, was equipped with azipod units and MARINTEK stock propellers.

Table 2. Main parameters of the Aker Arctic ice basin (Wilkman et al., 2010).

| Parameters | Value |
|---|---|
| Length | 75 m |
| Width | 8 m |
| Water depth | 2.1-2.2 m |
| Water volume | 1300 m$^3$ |



Figure 4. An example of the maneuvering tests in level ice (Source: Aker Arctic model test, Leiviskä, 2011).

The forward ice-going performance tests were conducted in three different level ice sheets (0.5, 0.8, and 1.2 m full-scale) using a constant rate of propeller revolutions. The model was free to move in all degrees of freedom except sway and yaw. On each test day, floe ice and ridge tests followed the level ice experiments, where the performance in each ice regime was tested running both ahead and astern. Draft and trim were adjusted to acquire the best possible performance ($T_F = 8.0$ m and $T_A = 6.0$ m).

The maneuvering tests were conducted running ahead with constant propulsion power. For the turning circle evaluation the azipod units were turned to the target angles, and the vessel was allowed to turn. Three different azimuth angles were applied (15, 35, and 55°) using both 100 and 120% propulsion power. It should be emphasized that the ice basin is too narrow to complete each turning circle; thus, the test results are only indicative.

The purpose of the stationkeeping experiments was to acquire an indication of the load levels associated with the operational ice conditions. This was obtained by towing the completely fixed vessel through stationary managed broken ice-fields with constant velocity. Such a setup simulates drifting ice, where the ice load time-series is recorded by a load cell in the connection point between the vessel and the towing carriage. Four different relative ice drift directions were applied (0, 5, 10, and 20°) in both 90 and 100% ice concentrations.

The experimental data on forward ice-going performance and stationkeeping have been applied in Su et al. (2012, 2013) and Kjerstad et al. (2013), respectively, to investigate the icebreaking and DP-ice capability of the CIVArctic vessel. The focus in this paper is an extensive analysis of the icebreaking capability and maneuverability by considering random crack size generation in the numerical simulation.

### 3.2 Numerical modeling

The normal open water draft for the vessel is $T_F = T_A = 6.5$ m , the ice draft is $T_F = 8.0$ m , and $T_A = 6.0$ m (draft and trim were adjusted in the ice model test to obtain the best possible ice performance). Figure 5 features the icebreaking waterline of the CIVArctic vessel. Compared to a typical icebreaker (see Figure 6), the CIVArctic vessel has three additional icebreaking components: the bulbous bow and the two headboxes of the azimuth propulsors at the stern. As shown in Figures 7 and 8, when the vessel is running ahead, the bulbous bow can break the ice upwards; when the vessel is running astern the headboxes can break the ice downwards. Therefore, the bulbous bow and the headboxes are modeled separately and the simulated icebreaking patterns have been compared with the experimental results (Leiviskä, 2011). Different parameters were applied in a previous study (Su et al., 2012) to investigate the vessel's performance in both model ice and full-scale sea ice. In the present study, only the model ice is considered.
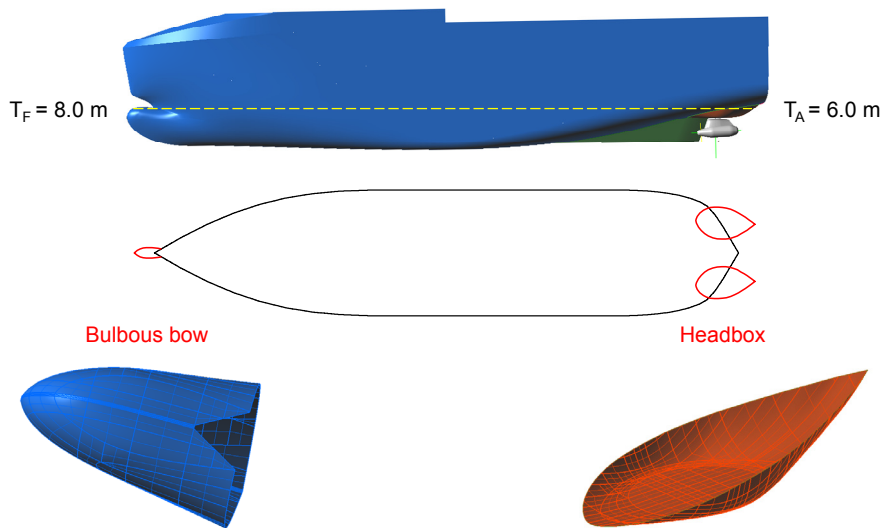


Figure 5. Icebreaking waterline of the CIVArctic vessel (double-acting vessel).
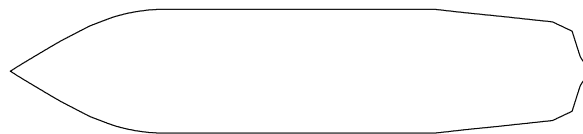


Figure 6. Icebreaking waterline of Tor Viking II (icebreaker, Riska et al., 2001).
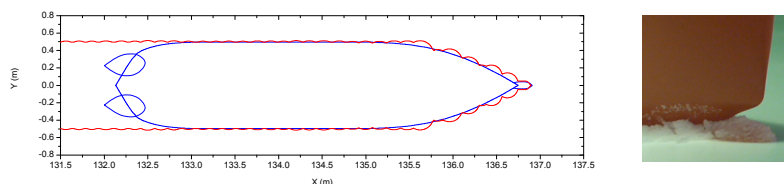


Figure 7. Icebreaking pattern around the bulbous bow in 22 mm (0.53 m full-scale) level ice.
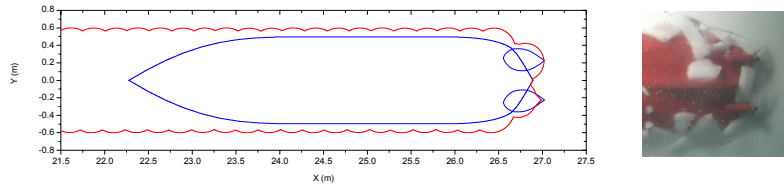
Figure 8. Icebreaking pattern around the headbox in 52 mm (1.26 m full-scale) level ice.

*Deterministic crack size*

In this study, the icebreaking pattern is firstly assumed to be determined by the characteristic length of ice, ship speed, and the frame angle around the hull. The bending crack is approximated by a circular arc and the crack radius is calculated by a deterministic expression given in Wang (2001) (based on information from Enkvist, 1972, and Varsta, 1983). It should be emphasized that the deterministic crack size does not mean the crack size is constant; it changes with the ice condition and ship's motion, but no random variation is included.

*Random crack size*

It is found in the model test that the ice is frequently crushed at the stem (with the bulb) when the vessel is running ahead. Sometimes bending failure also happens (as shown in Figure 9) and cracks of various sizes are observed in an icebreaking run (as shown in Figure 10). To the best of the author's knowledge, there is no reliable theory on the probabilistic distribution of the crack size during continuous icebreaking.
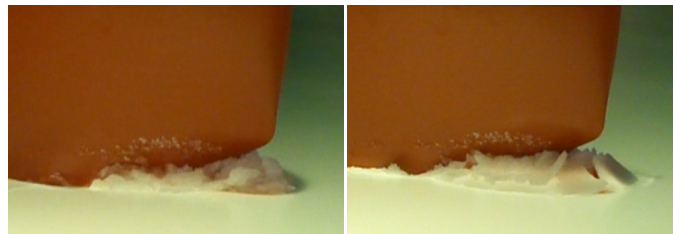


Figure 9. Screenshots from an icebreaking run in ice basin, running ahead in 22 mm (0.53 m full-scale) level ice.
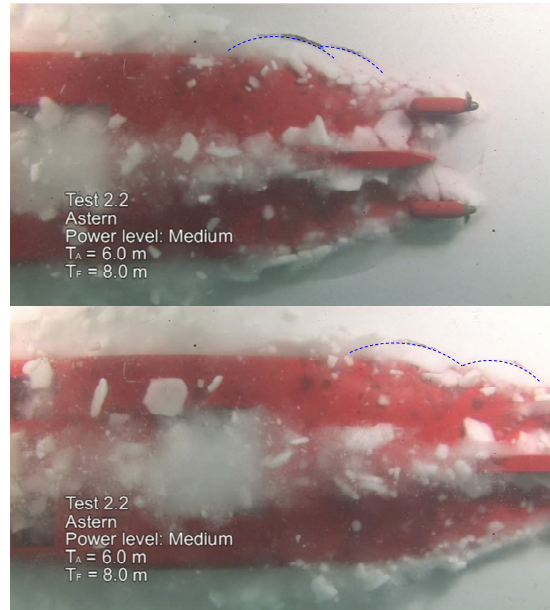
Figure 10. Screenshots from an icebreaking run in ice basin, running astern in 33 mm (0.80 m full-scale) level ice.

McKindra and Lutton (1981) analyzed the broken ice dimensions generated during the 1978-1979 winter ice trials of the U.S. Coast Guard 140-ft WTGB icebreaker. The hypothesis for this study was that the ice size distribution was log-normal. Tatinclaux (1986) also used the log-normal distribution on the floe size observed in the model tests of a wedge-shaped bow. In a numerical simulation of ice–cone interaction, Izumiyama et al. (1992) assumed that the crack size followed a normal distribution. As shown in Figure 11, the size of the crack is defined by the radius $R$ of the approximated circular arc and the ratio $Z$ of the crack radius to the length $l_{br}$, given by:

$$l_{br} = \left(\sigma_U h / \gamma\right)^{0.5} \qquad (9)$$

where $\sigma_U$ is the flexural strength of ice in upward bending, $h$ is the ice thickness, and $\gamma$ is the specific weight of water. The distribution has a mean $Z_m$ of 0.94 and a standard deviation $Z_{sd}$ of 0.27 which were determined based on the observed crack pattern in the model test. Izumiyama et al. (1992) gave no definite reason for the selection of normal distribution in this study. However, it was a reasonable estimate based on the experimental data.

In the present simulation, the crack size is defined by a random crack radius. There have been no reliable theory on the crack size distribution, and the available experimental data are not sufficient for a statistical analysis. Therefore, a normal distribution is used and the ratio between the standard deviation $R_{sd}$ and the mean crack radius $R_m$ is assumed to be the same as that shown in Figure 11 ($Z_{sd}/Z_m$). Herein, the mean crack radius is calculated by the deterministic method mentioned above (detailed expression can be found in Su et al. (2010a)). A random crack radius can then be generated by using:

$$F(R) = \frac{1}{\sqrt{2\pi \cdot R_{sd}}} \cdot \int_0^R \exp\left(\frac{-(s - R_m)^2}{2R_{sd}^2}\right) \cdot ds$$

$$U \sim U(0,1) \qquad\qquad\qquad\qquad (10)$$

$$R = F^{-1}(U)$$

where $F(R)$ is the cumulative distribution function (CDF) of the crack radius, $F^{-1}(U)$ is the inverse CDF, and $U$ is a randomly generated number between 0 and 1.

Figure 12 shows an example of the simulated icebreaking pattern with randomly generated crack sizes. In general, the numerical simulation is comparable to the experimental result, though the assumed circular crack can not capture all details of the observed icebreaking pattern. Differences do exist if we look at the instantaneous crack patterns. However, it is still a reasonable assumption for simulating the continuous icebreaking process and the ship's overall performance.



(a) Observed crack pattern

(b) Approximated crack pattern

(c) Crack size distribution
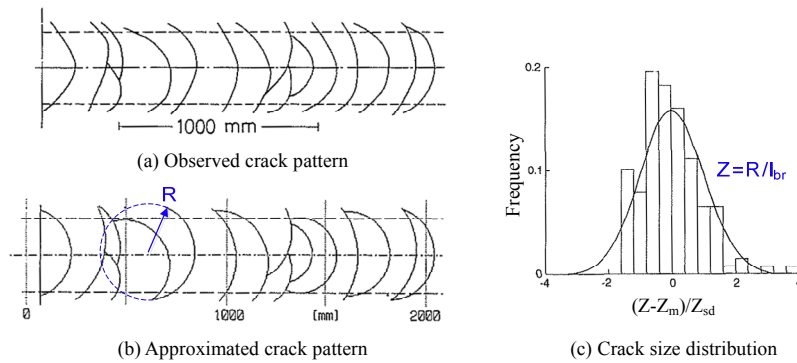
Figure 11. An example of the observed and approximated crack size distributions in the model test of ice–cone interaction (Courtesy: Izumiyama et al., 1992).
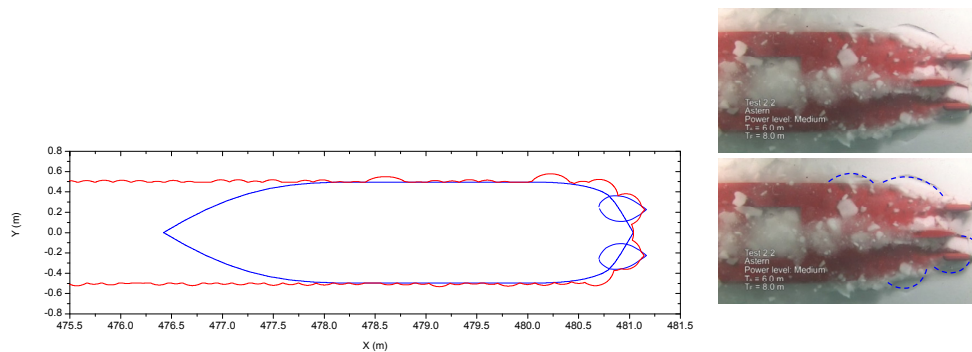


Figure 12. Simulated and observed icebreaking patterns, running astern in 33 mm (0.80 m full-scale) level ice.

*Propulsion*

The propulsion forces are applied to the vessel by using the thrust curves determined from model tests. It should be emphasized that only the two main stern propulsors are considered in the level-ice performance analysis. Different thrust curves are given in Leiviskä (2011) when the vessel is running ahead and astern. It is found that there is a reduction of net thrust when the vessel is running astern. In that case the ice resistance is also reduced

due to the flushing effect of the propeller jet which reduces the friction between the ship hull and ice. When running astern the propeller accelerates the water, which also makes the breaking of the ice easier (Vocke et al., 2011). The focus of this numerical model is on ice–hull interaction. Neither propeller jet nor propeller–ice interaction is included. The thrust deduction is taken into account by using the different ahead and astern thrust curves obtained in the open-water model tests. The flushing effect is simply accounted for by modifying the hull surface area covered by underwater broken ice pieces, which is based on the Lindqvist's (1989) formula of submerging and sliding ice resistance. This simplified method was introduced in Su (2012) and further discussed in Tan (2014) by comparing with the corresponding model test results.

## 4. Icebreaking capability analysis

The icebreaking capability is analyzed based on the experimental data and the simulated $h$ - $v$ curve. This displays the speed ($v$) that the vessel can attain in level ice as a function of the ice thickness ($h$). For direct comparison between the experimental data and the numerical model, the simulations required to create an $h$ - $v$ curve are conducted at model scale. The simulation results corresponding to deterministic and random crack sizes are then discussed.

### 4.1 Deterministic crack size

Figure 13 shows the $h$ - $v$ curves obtained when the vessel is running straight ahead and astern with deterministic crack size. A quadratic regression line is fitted to the simulation results and evaluated against the speed value obtained from the ice model test. For the ahead $h$ - $v$ curve, the single experimental data point fits the regression line nicely. As there is only one experimental data point, no regression line can be fitted to the experimental data for further investigation. The same procedure is applied to obtain the $h$ - $v$ curve running astern, which is also featured in Figure 13. In this case, two experimental speed values are available, and they are evenly distributed on both sides of the fitted simulation data line. Due to the limited experimental data, no regression line is fitted to the experiment.

The simulation results generally agree with the design intention that the level-ice-breaking capacity of the vessel should be better running astern (maximum ice thickness: 50 mm) than running ahead (maximum ice thickness: 24 mm). When the ship is running ahead, as shown in Figure 14 (a-b), the ice is frequently crushed at the stem (with the bulb) without bending failure, which is associated with high loads. As the bulb and bow are designed for open-water operations, they are found to be unfavorable for performance in level ice. A reason for the superior stern ice-handling capacity is shown in Figure 14 (c), where the ship is running astern, in which case the headboxes of the stern propulsors will interact and break the ice mainly through bending failure.
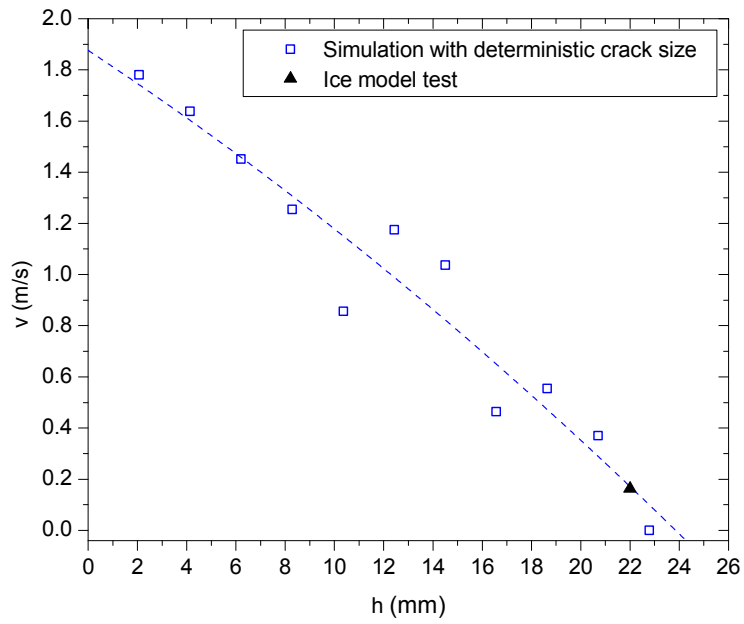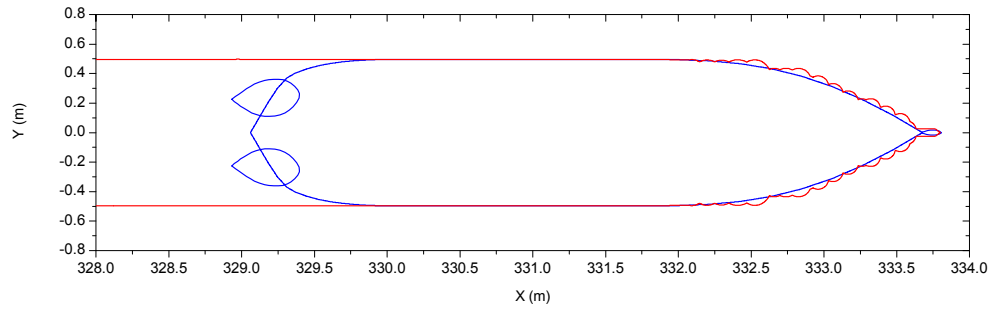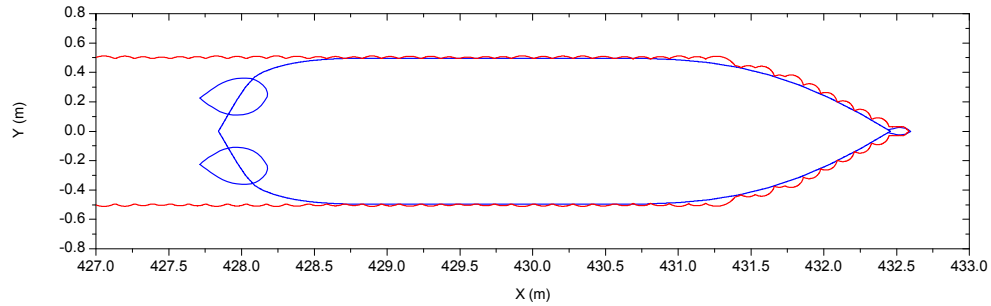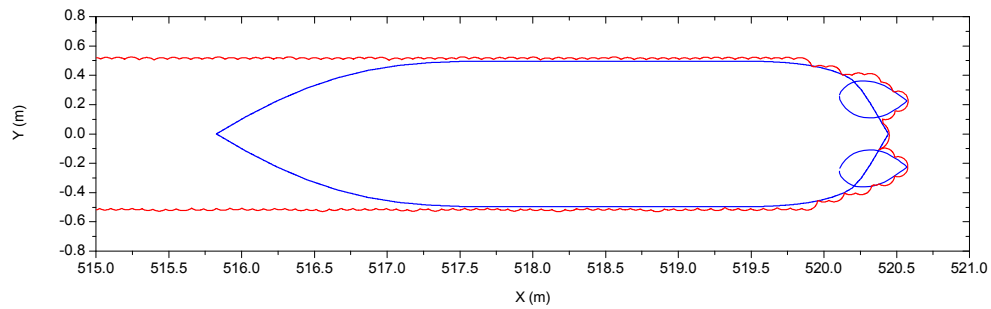
(a)
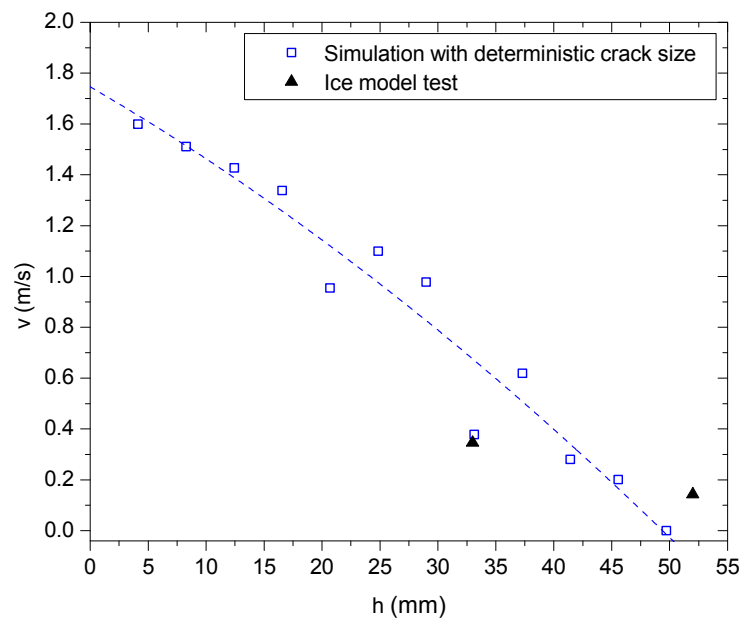


(b)

Figure 13. (a) $h$ - $v$ curve obtained when the vessel is running ahead. (b) $h$ - $v$ curve obtained when the vessel is running astern. All numbers are at model scale, and simulations are conducted with deterministic crack size.
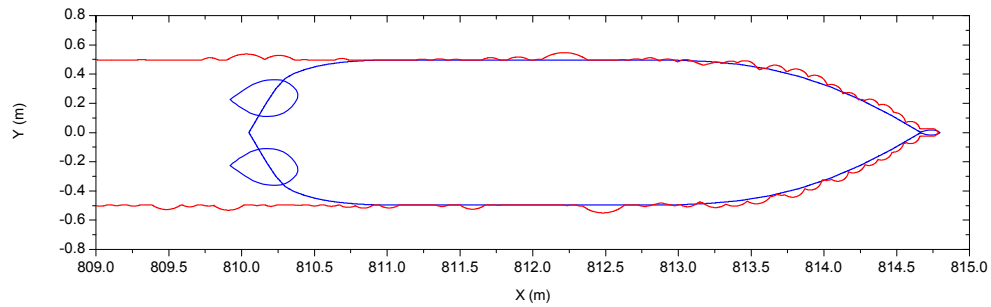
Figure 14. Examples of the simulated icebreaking runs with deterministic crack size. (a) Running ahead in 10.36 mm (0.25 m full-scale) level ice, featuring consistent shoulder crushing. (b) Running ahead in 12.43 mm (0.30 m full-scale) level ice. (c) Running astern in 12.43 mm (0.30 m full-scale) level ice.

Another finding from the numerical simulation is the presence of so-called shoulder crushing. The CIVArctic vessel is designed to have a vertical hull surface at the midship and a large slope angle (close to 90°) at the shoulder area. Therefore, the hull shoulder can not break the ice by bending, and shoulder crushing happens when the bow or the stern breaks a narrower channel than the ship beam. In this case the ship has to force itself to crush the rest of the channel width close to the ship beam, and the ice resistance is highly increased. As shown in Figure 14 (a), shoulder crushing consistently happens during the simulated icebreaking run in 10.36 mm (0.25 m full-scale) level ice. Accordingly, the obtained speed of the ship is lower than in the cases without consistent shoulder crushing, even in the cases in which the ice is thicker (e.g., 12.43 and 14.50 mm as shown in Figure 13 (a)).

**4.2 Random crack size**

Figure 15 shows two examples of the simulated icebreaking runs with random crack size. Compared with Figure 14, an obvious time-variation of the crack pattern can be found during one icebreaking run (in a certain ice condition). But the variation from one ice condition to another is reduced if we look at the shoulder crushing effect. As shown in Figure 15, intermittent shoulder crushing is observed in both 10.36 and 12.43 mm ice, while Figure 14 shows consistent shoulder crushing in 10.36 mm ice but almost no shoulder crushing in 12.43 mm ice.



(a)
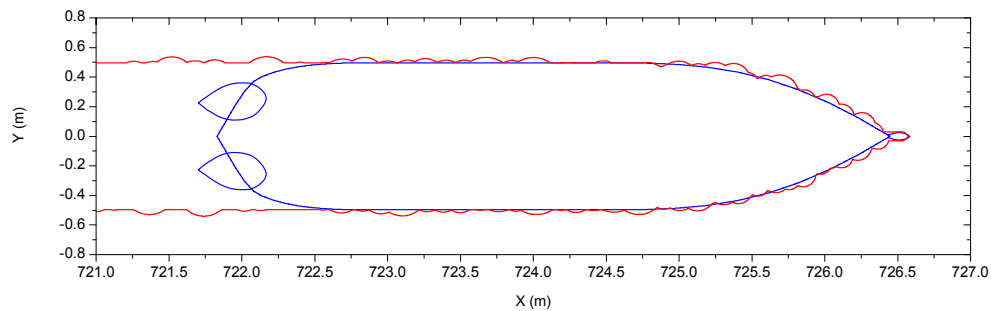


(b)

Figure 15. Examples of the simulated icebreaking runs with random crack size. (a) Running ahead in 10.36 mm (0.25 m full-scale) level ice. (b) Running ahead in 12.43 mm (0.30 m full-scale) level ice.

Figure 16 shows a comparison between the simulated velocity time-series in 10.36 mm ice and Figure 17 shows the comparison in 12.43 mm ice. When the random crack size is applied, it is found that the simulated ship speed in 10.36 mm ice is increased due to a decreased effect of shoulder crushing (from consistent to intermittent), while the simulated ship speed in 12.43 mm ice is decreased due to the occurrence of shoulder crushing (from no shoulder crushing to intermittent shoulder crushing). If the shoulder crushing only happens in 10.36 mm ice, the simulated ship speed in this ice condition is even lower than in 12.43 mm ice. As shown by Figures 16 and 17, this variation will disappear if the shoulder crushing happens in both 10.36 and 12.43 mm ice.

Figure 18 shows a comparison of the simulated ice force (in surge direction) time-series in 12.43 mm ice. The blue line features the result in which the deterministic crack size is applied while the red line features the result in which the random crack size is applied. The difference between these two results reflects the shoulder crushing effect. It is found that the ice resistance in a short time period (see e.g. the time period from 191 to 192

s) is increased by about 45% due to the occurrence of shoulder crushing. In general, the average ice resistance (from 100 to 300 s) is increased by about 21%, and this results in a 16% decrease of ship speed (as shown in Figure 17).

The simulated $h$ - $v$ curves are compared in Figure 19. It is found that when the random crack size is applied the simulation results are more smoothly distributed along the fitted regression line. This is because the shoulder crushing happens in almost all ice conditions in a moderate manner. In general, by introducing a random variation of the crack size the numerical model will give a more consistent evaluation of the ship's performance in various ice conditions. The deterministic icebreaking pattern, on the other hand, may reveal a limit state in a certain ice condition. As shown in Figure 16 (a), the simulated ship speed is decreased by about 23% when consistent shoulder crushing happens.



(a)



(b)
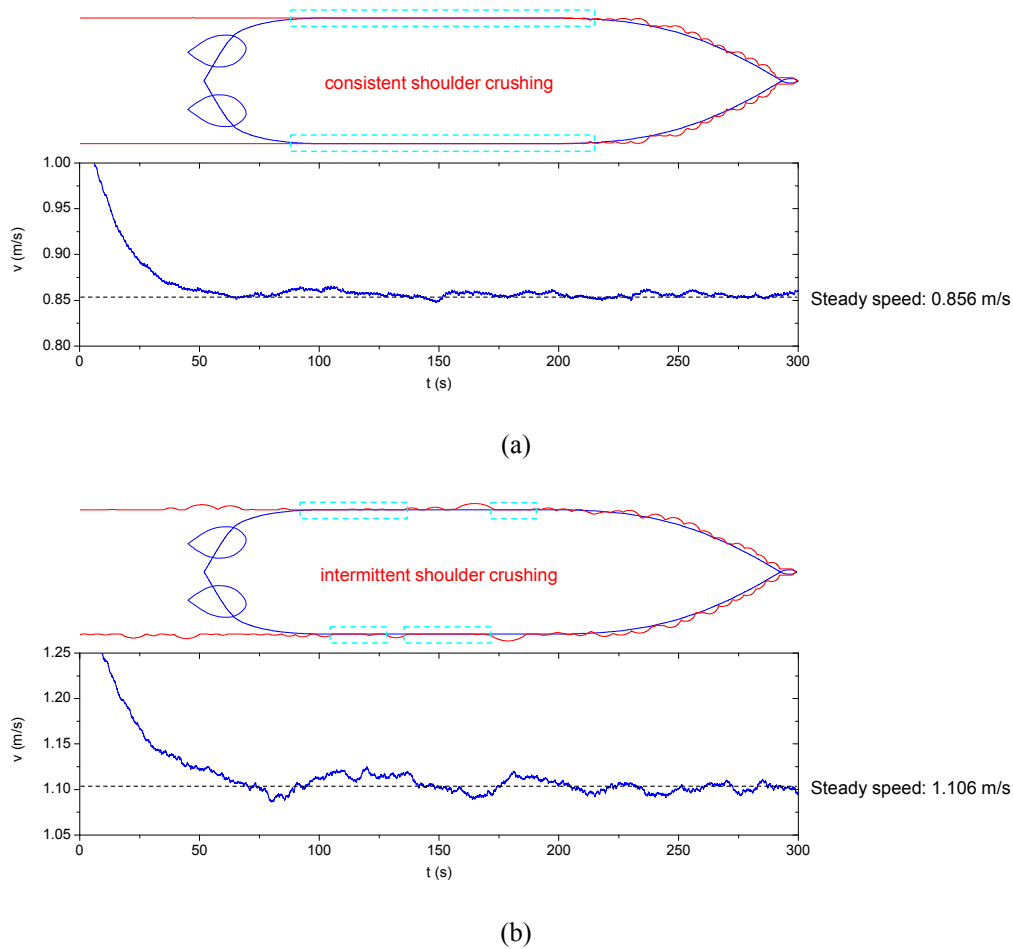
Figure 16. Comparison between the simulated velocity responses. (a) Deterministic crack size. (b) Random crack size. Running ahead in 10.36 mm (0.25 m full-scale) level ice.
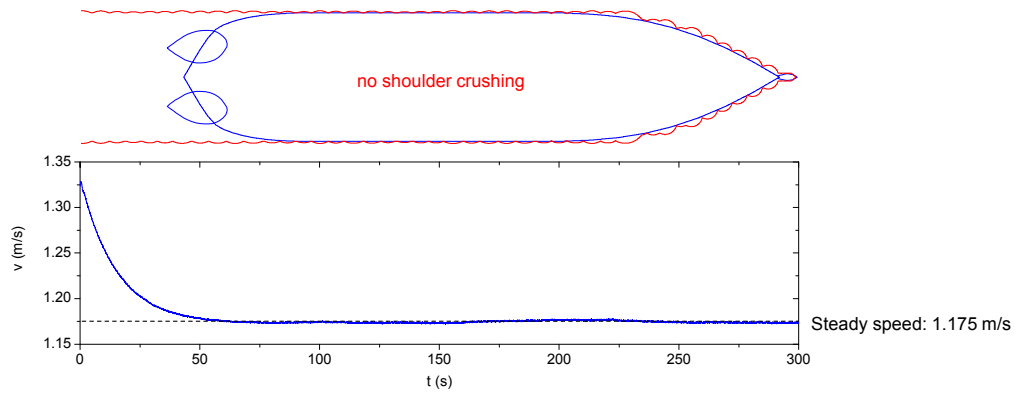
(a)
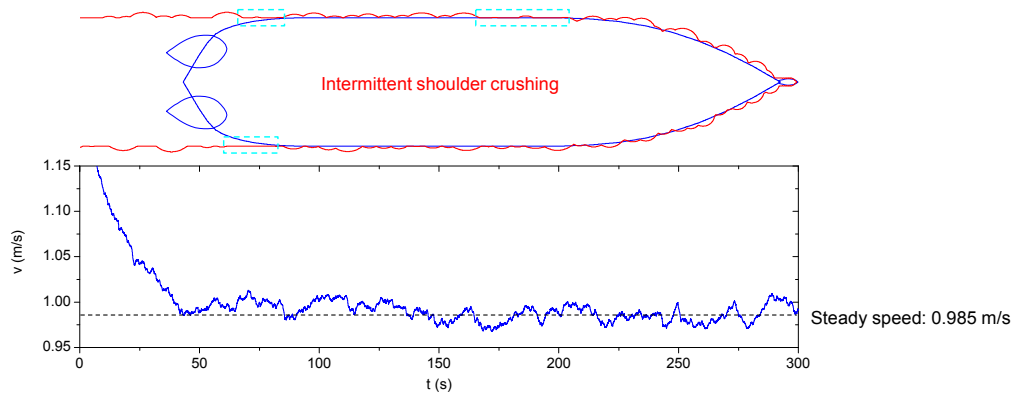


(b)

Figure 17. Comparison between the simulated velocity responses. (a) Deterministic crack size. (b) Random crack size. Running ahead in 12.43 mm (0.30 m full-scale) level ice.
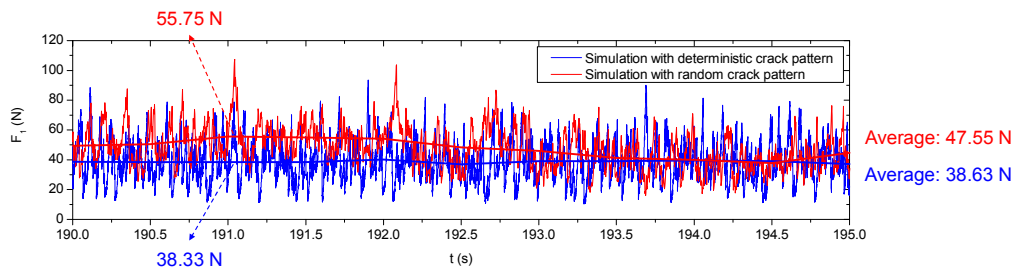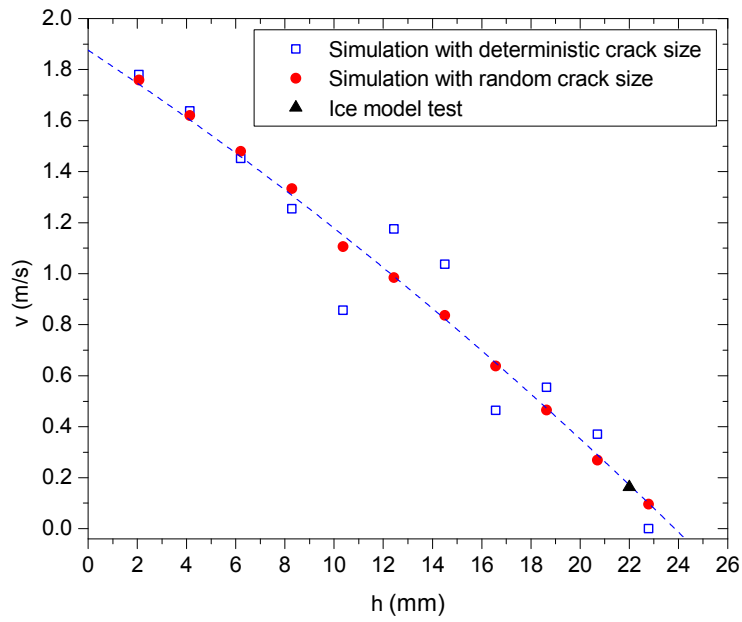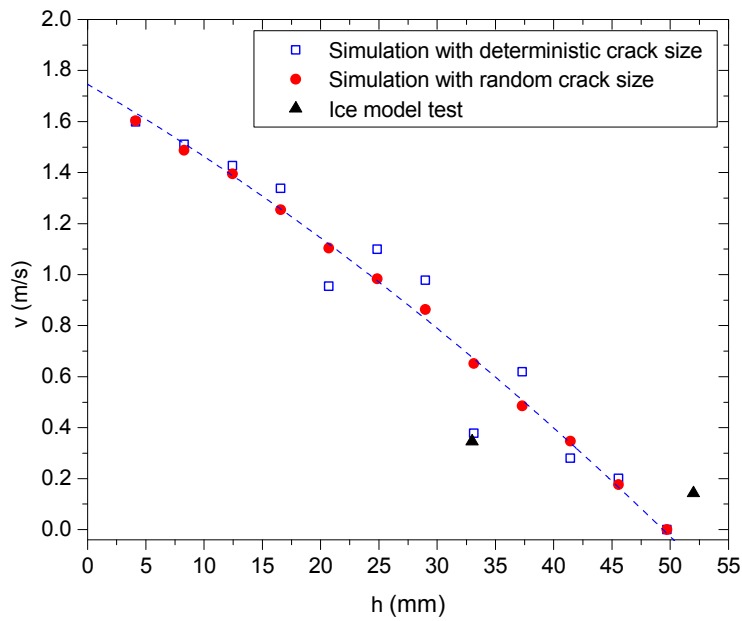


Figure 18. Comparison between the simulated ice force (in surge direction) time-series, running ahead in 12.43 mm (0.30 m full-scale) level ice with deterministic and random crack size.

(a)



(b)

Figure 19. (a) $h$ - $v$ curve obtained when the vessel is running ahead. (b) $h$ - $v$ curve obtained when the vessel is running astern. All numbers are at model scale, and simulations are conducted with deterministic and random crack size.

## 5. Maneuverability analysis

The maneuverability of the CIVArctic vessel in level ice is analyzed based on the experimental data and the simulated turning circles. The simulations required to evaluate the turning circle diameters are conducted at

model scale and the random crack size is applied. The turning performance is then measured by the turning circle diameter ( $D_t$ ) divided by the ship length ( $L$ ).

During the turning tests conducted in the Aker Arctic ice basin, three different propulsion azimuth angles were applied (15, 35, and 55°), and 120% power was used in all cases but one, where 100% was used. The reason for the high power level was that the vessel was already struggling when approaching directly ahead in the 19.7 mm (0.5 m full-scale) level ice sheet used for the turning tests. Figure 20 shows the setup of each test and the measured turning tracks. Since the Aker Arctic ice basin is too narrow to complete each turning circle, the turning diameter was roughly estimated by a circular regression of the measured turning tracks (Leiviskä, 2011).
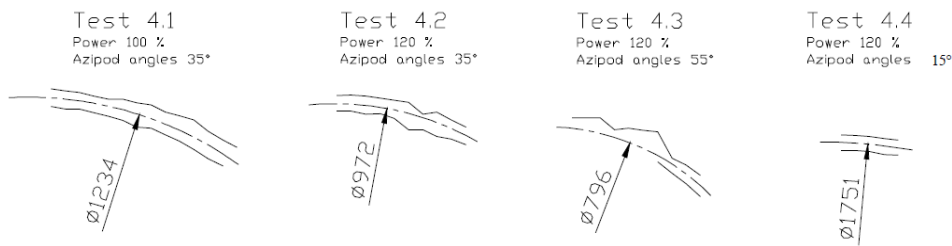


Figure 20. The measured tracks and estimated turning diameters from the model tests (Source: Aker Arctic model test, Leiviskä, 2011). All numbers are at full scale (in meters).

Figure 21 shows the simulated turning circle using 120% power and a propulsion azimuth angle of 35°. The vessel loses velocity when turning, and the simulated turning circle diameter is about $20L$. This is much higher than the $5L$ requirement for vessels that have to maneuver well in certain ice conditions (Riska, 2010). By increasing the propulsion azimuth to 55°, the vessel still does not turn well, and both model tests (Leiviskä, 2011) and previous simulation results have shown that the vessel can eventually get stuck in the ice (as shown in Figure 22).
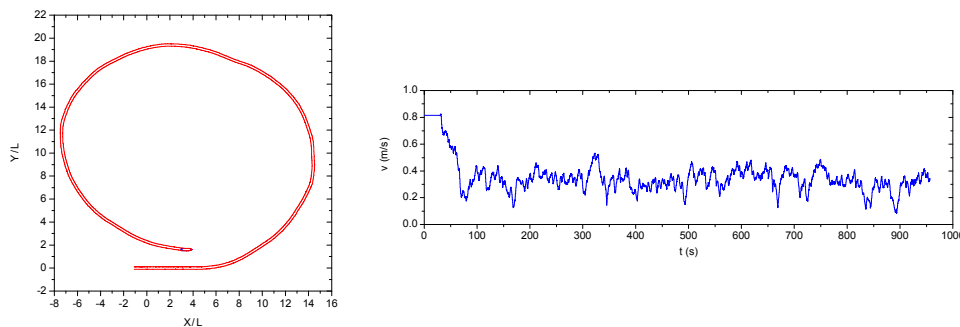


Figure 21. Simulated turning circle in 19.7 mm (0.5 m full-scale) level ice (power 120%, azimuth angle 35°) with the corresponding velocity response. The turning circle is plotted with reference to ship length $L$.
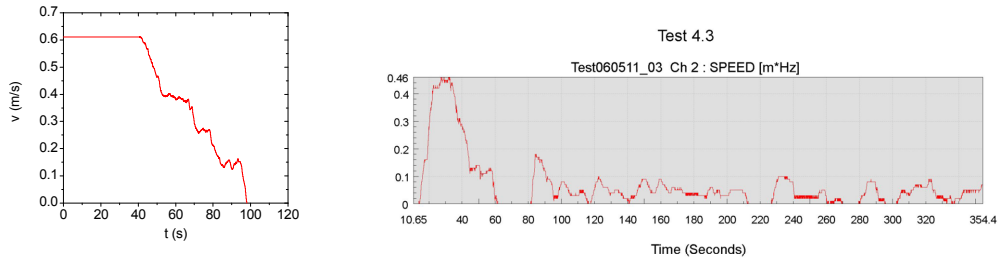
Figure 22. Simulated (left) and measured (right) velocity time-series in 19.7 mm (0.5 m full-scale) level ice (power 120%, azimuth angle 55°).

As shown in Figure 23, an inward heel of the vessel was observed in the model tests and the estimated average heeling angle is around 2°. This is also considered in the numerical simulation. As shown in Figure 24, the changed icebreaking waterline and hull angles are determined from a three-dimensional model of the vessel. Then Figure 25 shows the comparison between the numerical simulation and experimental results. A 2° heeling angle and the different ice thicknesses are applied in the numerical simulations. However, the available experimental data are not sufficient for a meaningful comparison.
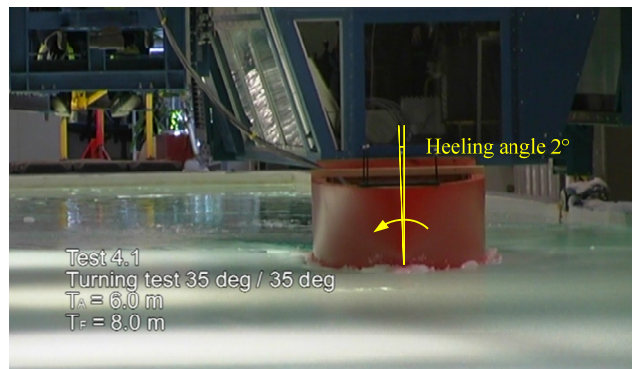


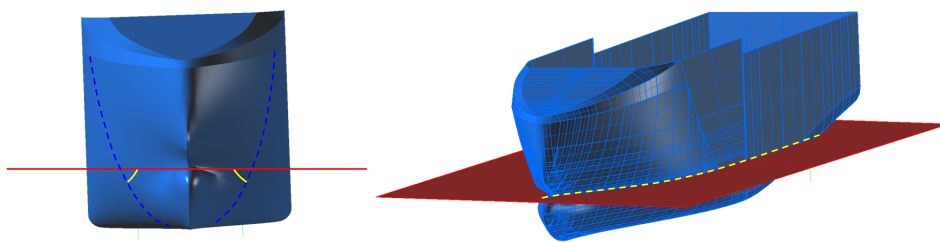Figure 23. Estimated average heeling angle during the turning test.



Figure 24. Changed icebreaking waterline and hull angles by considering an inward heel of the vessel.
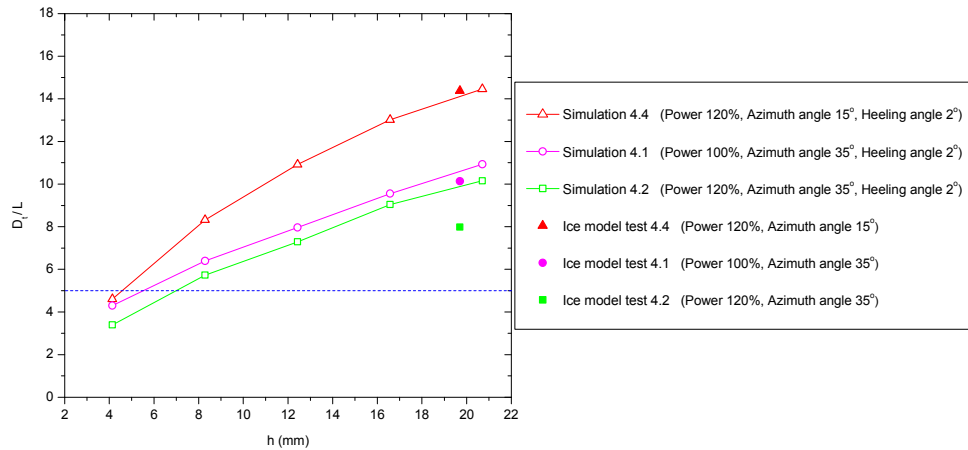
Figure 25. Comparison between the simulated turning circle diameters and the estimated values from the model tests. The turning circle diameter $D_t$ is divided by ship length $L$. All numbers are at model scale.

A parameter study of the heeling angle is then shown in Figure 26. On average the turning circle diameter is reduced by about 65% when a 3° heeling angle is applied. This conclusion is based on a numerical study with a specific hull form. As shown in Figure 27, the inward heel of the vessel makes its port side break ice in a more favorable way. As mentioned before, the CIVArctic vessel has a vertical hull surface at the midship which can not break the ice by bending when the vessel is upright. By heeling the vessel, large bending cracks are created at the midship and aft shoulder areas, resulting in a better turning performance. However, the conclusions may be different if the hull forms are different. For example, during the field trials of the icebreaker Tor Viking II (Riska et al., 2001), it was found that when a 3° heeling angle was applied, the turning circle diameter of the vessel was only reduced by about 42% (in 0.6 m level ice).
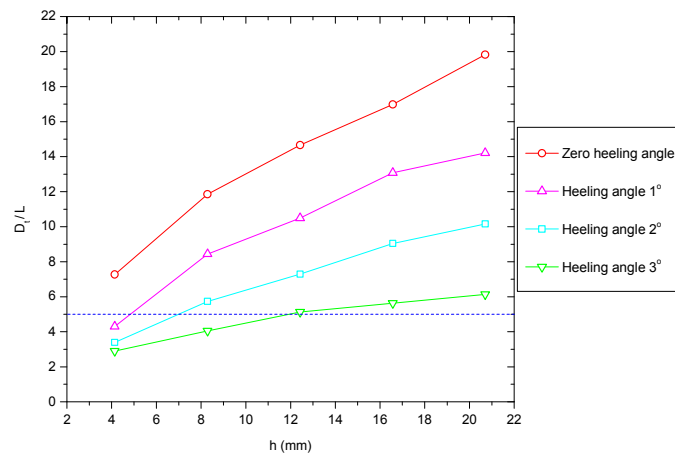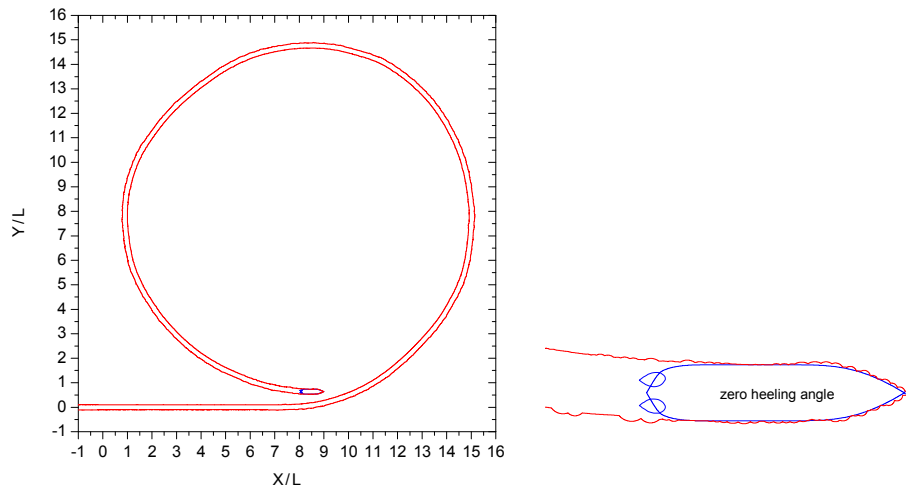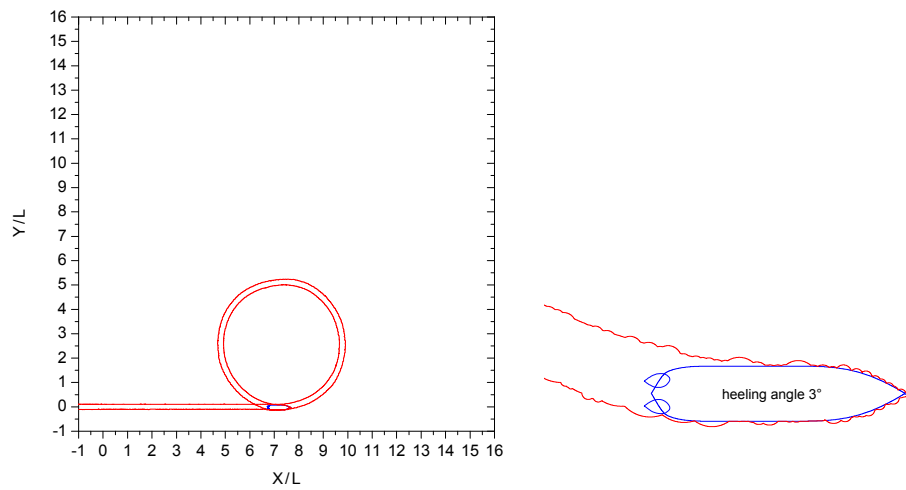


Figure 26. Simulated turning circle diameters in different ice conditions (power 120%, azimuth angle 35°). The turning circle diameter $D_t$ is divided by ship length $L$. All numbers are at model scale.

Figure 27. Simulated turning circles in 12.43 mm (0.3 m full-scale) level ice (power 120%, azimuth angle 35°). (a) Zero heeling angle. (b) Heeling angle 3°. The turning circle is plotted with reference to ship length $L$.

Figure 28 shows also a simulated turning circle when the CIVArctic vessel is running astern with zero heeling angle. It is found that the turning performance of the vessel is better when it is running astern than when it is running ahead, as shown in Figure 29, where the turning circle diameter is reduced by about 30% on average. This conclusion is solely based on the simulation results since no experimental data are available for comparison.
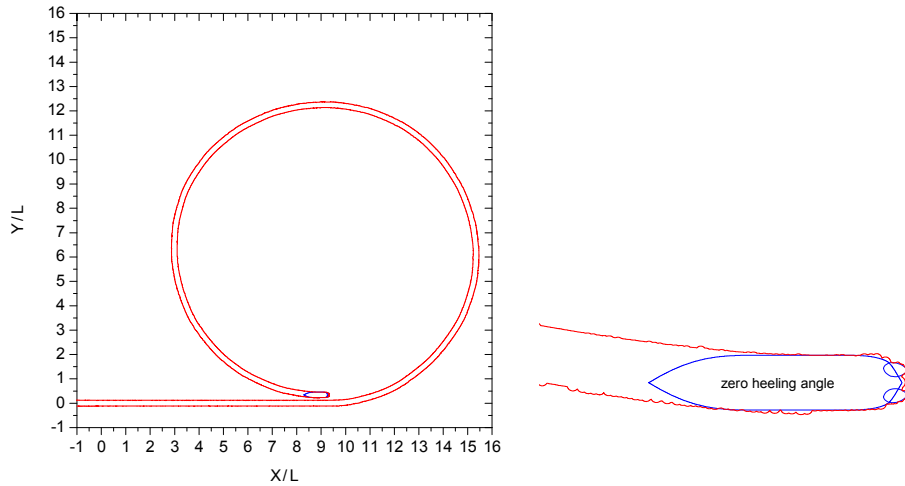
Figure 28. Simulated astern turning circle in 12.43 mm (0.3 m full-scale) level ice (power 120%, azimuth angle 35°). The turning circle is plotted with reference to ship length $L$.
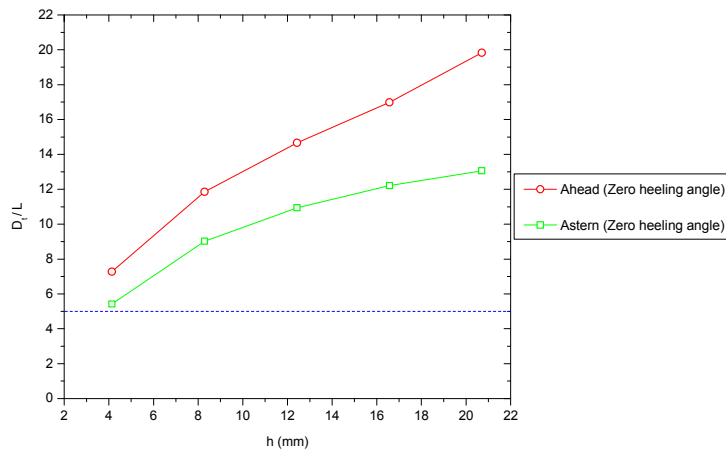


Figure 29. Comparison between the ahead and astern turning circles (power 120%, azimuth angle 35°). The simulated turning circle diameter $D_t$ is divided by ship length $L$.

## 6. Conclusions

In this paper, a numerical model is used to investigate the level ice performance of a double-acting intervention vessel designed mainly for open water. The simulation results are consistent with the design intention that the stern should have enhanced ice handling capabilities compared to the bow. The reason lies in the open-water design, as ice is mainly crushed when moving ahead instead of breaking by a more efficient failure mode. Another contributor to this performance gap lies in the headboxes of the main propulsors, as these provide favorable interaction with the ice sheet, catering for more efficient icebreaking.

The numerical simulation results are not only compared with the experimental data for validation. They also provide more information about the continuous icebreaking process and its effect on the vessel's performance in different ice conditions and modes of operations.

In terms of forward ice-going performance, it is found that the occurrence of shoulder crushing can cause increased ice resistance, which may considerably impair the ship's performance in certain ice conditions. When a random variation of the crack size is considered in the numerical simulations, intermittent shoulder crushing is observed in almost all ice conditions. This will give a more consistent evaluation of the ship's performance in various ice conditions, as seen in the corresponding $h$ - $v$ curves.

In terms of maneuvering, it is found that the turning performance of the vessel can be improved if an inward heel of the vessel is allowed. On average, the numerical simulations indicate that the turning circle diameter is reduced by 65% if a 3° heeling angle is applied. It is also found that the turning circle diameter is reduced by about 30% when the vessel is operated stern first. The available experimental data are unfortunately not sufficient for a valid comparison with the numerical simulation results. Therefore these conclusions should be further investigated if more experimental data becomes available.

In general, the numerical simulation results can supplement the experimental data by providing more information about the vessel's maneuverability in level ice and identifying the physical foundation for the exhibited performance of the vessel. However, limitations do exist in both numerical simulations and ice model tests. The propeller jet and propeller–ice interaction are not included in the numerical model, and some assumptions are made, including the approximated circular crack, normal distribution of the crack size, and decomposition of the ice resistance. The model test results are influenced by many parameters, such as the type of the model ice, size of the ice basin relative to the model, and possible edge effects. Regarding these issues, further studies and accumulation of data are required.

**References**

Berg, T.E., Berge, B.O., Borgen H., Hänninen, S., Suojanen, R.A., Su, B., 2013. Offshore vessel design for Barents Sea operations. Proc. 21st Int. Conf. Port and Ocean Engineering under Arctic Conditions (POAC 2013), Espoo, Finland.

Enkvist, E., 1972. On the Ice Resistance Encountered by Ships Operating in the Continuous Mode of Icebreaking. Report No.24, Swedish Academy of Engineering Science in Finland, Helsinki, Finland.

Enkvist, E., Varsta, P., Riska, K., 1979. The ship–ice interaction. Proc. 5th Int. Conf. Port and Ocean Engineering under Arctic Conditions (POAC 1979), pp. 977–1002.

Faltinsen, O.M., 1990. Sea Loads on Ships and Offshore Structures. Cambridge University Press, Cambridge, UK.

Izumiyama, K., Kitagawa, H., Koyama, K., Uto, S., 1992. A numerical simulation of ice–cone interaction. Proc. 11th Int. Symp. Ice (IAHR 1992), Banff, Alberta.

Jones, S.J., 2004. Ships in ice—a review. 25th Symp. Naval Hydrodynamics, St. John's, Newfoundland and Labrador, Canada, August 2004.

Juva, M., Riska, K., 2002. On the Power Requirement in the Finnish–Swedish Ice Class Rules. Research Report No. 47. Technical report, Winter Navigation Research Board, Finland and Sweden.

Kjerstad, Ø. K., Metrikin, I., Løset, S. and Skjetne R., 2014. Experimental and phenomenological investigation of dynamic positioning in managed ice. Submitted to Cold Reg. Sci. Technol.

Kjerstad, Ø.K., Skjetne, R., Berge, B.O., 2013. Constrained nullspace-based thrust allocation for heading prioritized stationkeeping of offshore vessels in ice. Proc. 22nd Int. Conf. Port and Ocean Engineering under Arctic Conditions (POAC 2013), Espoo, Finland.

Leiviskä, T., 2011. Performance and DP Tests in Ice with CIVArctic Vessel. AARC Report A-454. Technical report, Aker Arctic.

Lindqvist, G., 1989. A straightforward method for calculation of ice resistance of ships. Proc. 10th Int. Conf. Port and Ocean Engineering under Arctic Conditions (POAC 1989), Luleå, Sweden.

Liu, J., Lau, M., Williams, F.M., 2006. Mathematical modeling of ice–hull interaction for ship maneuvering in ice simulations. Proc. 7th Int. Conf. Exhib. Performance of Ships and Structures in Ice (ICETECH), Banff, Alberta, Canada.

Lubbad, R., Løset, S., 2011. A numerical model for real-time simulation of ship–ice interaction. Cold Reg. Sci. Technol., 65, 111–127.

Martio, J., 2007. Numerical Simulation of Vessels Maneuvering Performance in Uniform Ice. Report No. M-301. Technical report, Ship Laboratory, Helsinki University of Technology, Finland.

McKindra, C.D. and Lutton, T.C., 1981. Statistical analysis of broken ice dimensions generated during 140-ft WTGB icebreaking trials. Proc. 6th Int. Conf. Port and Ocean Engineering under Arctic Conditions (POAC 1981), Quebec, Canada.

Metrikin, I., Kerkeni, S., Jochmann, P., Løset, S., 2013. Experimental and numerical investigation of dynamic positioning in level ice. Proc. 32nd Int. Conf. Offshore Mechanics and Arctic Engineering (OMAE 2013), Nantes, France.

Newmark, N.M., 1959. A method of computation for structural dynamics. J.. Eng. Mech. Div., ASCE, 85, 67–94.

Nguyen, D.T., Sørbø, A.H., Sørensen, A.J., 2009. Modelling and control for dynamic positioned vessels in level ice. Proc. Conf. Manoeuvring and Control of Marine Craft, pp. 229–236.

Riska, K., 2007. Application of the SAFEICE project results in developing the Finish Swedish ice class rules. Report for Deliverable D7-3 of SAFEICE Project, December 2007.

Riska, K., 2010. Ship–ice Interaction in Ship Design: Theory and Practice. Encyclopedia of Life Support Systems (EOLSS), Developed under the Auspices of the UNESCO, Eolss Publishers, Oxford, UK, [http://www.eolss.net].

Riska, K., Wilhelmson, M., Englund, K., Leiviskä, T., 1997. Performance of Merchant Vessels in Ice in the Baltic. Research Report NO. 52. Ship Laboratory, Helsinki University of Technology.

Riska, K., Leiviskä, T., Nyman, T., Fransson, L., Lehtonen, J., Eronen, H., Backman, A., 2001. Ice performance of the Swedish multi-purpose icebreaker Tor Viking II. Proc. 16th Int. Conf. Port and Ocean Engineering under Arctic Conditions (POAC 2001), Ottawa, Canada.

Sawamura, J., Tsuchiya, H., Tachibana, T., Osawa, N., 2010. Numerical modeling for ship maneuvering in level ice. Proc. 20th Int. Symp. Ice (IAHR 2010), Lahti, Finland.

Su, B., 2012. Full-scale and model scale simulations of the level ice performance of CIVArctic vessel. Report No. 530529, MARINTEK, Trondheim, Norway.

Su, B., Riska, K., Moan, T., 2010a. A numerical method for the prediction of ship performance in level ice. Cold Reg. Sci. Technol., 60, 177–188.

Su, B., Riska, K., Moan, T., 2010b. Numerical simulation of ship turning in level ice. Proc. 29th Int. Conf. Offshore Mechanics and Arctic Engineering (OMAE 2010), Shanghai, China.

Su, B., Riska, K., Moan, T., 2011. Numerical simulation of local ice loads in uniform and randomly varying ice conditions. Cold Reg. Sci. Technol., 65, 145–159.

Su, B., Riska, K., Moan, T., Berg, T.E., 2012. Full-scale and model-scale simulations of a double acting intervention vessel operating in level ice. Proc. 21st IAHR Int. Symp. Ice (IAHR 2012), Dalian, China.

Su, B., Kjerstad, Ø.K., Skjetne, R., Berg, T.E., 2013. Ice-going capability assessment and DP-ice capability plot for a double acting intervention vessel in level ice. Proc. 22nd Int. Conf. Port and Ocean Engineering under Arctic Conditions (POAC 2013), Espoo, Finland.

Tan, X., Su, B., Riska, K., Moan, T., 2013. A six-degrees-of-freedom numerical model for level ice–ship interaction. Cold Reg. Sci. Technol., 92, 1–16.

Tan, X., 2014. Numerical investigation of ship's continuous-mode icebreaking in level ice. Doctoral Thesis, Department of Marine Technology, Norwegian University of Science and Technology, Norway.

Tatinclaux, J.C., 1986. Ice floe distribution in the wake of a simplified wedge. Proc. 15th Int. Conf. Offshore Mechanics and Arctic Engineering (OMAE 1986), Tokyo, Japan.

Valanto, P., 2001. The resistance of ships in level ice. Trans. Soc. Nav. Archit. Mar. Eng. (SNAME), 109, 53–83.

Varsta, P., 1983. On the mechanics of ice load on ships in level ice in the Baltic Sea. Publications 11, Technical Research Centre of Finland, Espoo, Finland.

Vocke, M., Ranki, E., Uuskallio, A., Niini, M., Wilkman, G., 2011. Experience from vessels operating in ice in the double acting principle. Proc. Arctic Technology Conf. 2011, Houston, Texas, USA.

Wang, S., 2001. A dynamic model for breaking pattern of level ice by conical structures. Doctoral Thesis, Department of Mechanical Engineering, Helsinki University of Technology, Finland.

Wilkman, G., Forsén, A.C., Mattsson T., 2010. Recent advancements in ice model testing at Aker Arctic. Proc. 20th IAHR Int. Symp. Ice (IAHR 2010), Lahti, Finland.